6. T. L. James, *Curr. Opin. Struct. Biol.* **1**, 1042 (1991).
7. A. M. J. J. Bonvin, R. Boelens, R. Kaptein, in *Computer Simulation of Biomolecular Systems: Theoretical and Experimental Applications*, vol. 2, W. F. van Gunsteren, P. K. Weiner, A. J. Wilkinson, Eds. (ESCOM Science, Leiden, Netherlands, 1993).
8. M. Stone, *J. R. Stat. Soc. Ser. B* **36**, 111 (1974); B. Efron, *The Jackknife, the Bootstrap, and Other Resampling Plans* (Society for Industrial and Applied Mathematics, Philadelphia, PA, 1982); B. Efron, *SIAM Rev.* **30**, 421 (1988).
9. A. T. Brunger, *Nature* **355**, 472 (1992); *Acta Crystallogr. Sect. D* **49**, 24 (1993).
10. Complete cross-validation consisted of a random partitioning of the distance data (*16*) into 10 sets of roughly equal size. Ten working sets were defined that excluded each one of the test sets from the full distance data set, one at a time. Structure determinations with a hybrid distance geometry and SA protocol (*12*) were performed with each of the working sets. A structure was accepted if the distance bound violation for the working set was less than 1 Å and the dihedral angle violation less than 10°. If one of these conditions was violated, the protocol was repeated with the same working set but different initial conditions (random number seed for distance geometry and initial velocities for SA) until the conditions were satisfied. Statistical quantities, such as distance bound violations, were averaged over the successful runs. Complete cross-validation was repeated with eight different partitionings of the data set and the statistical quantities averaged.
11. B. R. Brooks *et al.*, *J. Comput. Chem.* **4**, 187 (1983); A. T. Brunger, *Annu. Rev. Phys. Chem.* **42**, 197 (1991).
12. A hybrid distance-geometry and SA method (*24*) was used to determine conformations of the molecule consistent with both the experimental data and the chemical restraints (Eq. 1). The SA stage reduces bias attributable to insufficient sampling during the distance-geometry stage. Metric matrix distance geometry was applied to substructures consisting of Cα, Hα, N, HN, C, Cβ, and Cγ atoms (*25*). The coordinates of all atoms of a particular residue were then set to the coordinates of template structures fitted to the substructure coordinates (*24*). The resulting all-atom model was optimized by SA. The energy constants, the van der Waals radii, and the temperature were varied during SA to achieve best convergence as described in X-PLOR, protocol DGSA (*24, 26*). The geometric energy function E_{chemical} (Eq. 1) used the "parallhdg.pro" parameters in X-PLOR, version 3.1 (*26*), with the following final values for the conformational energy constants: 1000 kcal mol^{-1} Å^{-2} for bond terms and 500 kcal mol^{-1} rad^{-2} for angle and improper terms. The van der Waals potential was described by a quartic repulsive potential (*24*) with the hard-sphere radii set to 0.75 times their standard values in "parallhdg.pro" and an energy constant of 4 kcal mol^{-1} Å^{-2}. The final value for the energy constant w_{torsion} (Eq. 1) was set to 200 kcal mol^{-1} rad^{-2}.
13. T. F. Havel and K. Wüthrich, *J. Mol. Biol.* **182**, 281 (1985).
14. G. M. Clore, M. A. Robien, A. M. Gronenborn, *ibid.* **231**, 82 (1993).
15. A. M. Gronenborn *et al.*, *Science* **253**, 657 (1991).
16. The observed distance data set consisted of 854 distance restraints derived from NOE experiments and 68 distance restraints for 34 hydrogen bonds involving slowly exchanging backbone amide protons (*15*). The former contained 291 long-range interresidue restraints ($|i - j| > 5$ for residue numbers i,j) that determine the tertiary fold of the structure. In addition, 105 torsion angle restraints derived from experimental NOE and three-bond coupling constant data were included in the calculations. All torsion angle restraints were used during cross-validation of the distance data set. The influence of these torsion angle restraints on the computed statistical quantities was less than a few percent because these rather generous restraints help convergence but have little influence on the final structures.
17. P. Yip and D. A. Case, *Chem. Phys. Lett.* **161**, 50 (1989).
18. P. D. Thomas, V. J. Basus, T. L. James, *Proc. Natl. Acad. Sci. U.S.A.* **88**, 1237 (1991); C. Gonzales, J. A. C. Rullmann, A. M. J. J. Bonvin, R. Boelens, R. Kaptein, *J. Magn. Reson.* **91**, 659 (1991); S. A. White, M. Nilges, A. Huang, A. T. Brunger, P. B. Moore, *Biochemistry* **31**, 1610 (1992); J. M. Withka, J. Srinivasan, P. H. Bolton, *J. Magn. Reson.* **98**, 611 (1992).
19. T. A. Holak, D. Gondol, J. Otlewski, T. Wilusz, *J. Mol. Biol.* **210**, 635 (1989).
20. M. Nilges, J. Habazettl, A. T. Brünger, T. A. Holak, *ibid.* **219**, 499 (1991).
21. We simulated a total of 425 NOE intensities at a mixing time of 150 ms using $\langle r^{-3}\rangle^{-1/3}$ averaging for methyl groups, uniform isotropic tumbling with a rotational correlation time of 2.3 ns, and a 4 Å cutoff (*20*) for the computation of the relaxation pathways. The structure termed "$cmti_1$" in (*20*) was used to calculate an intensity data set for NOEs that were actually observed for CMTI (*20*). Noise was added to the calculated data set with a uniform random number generator; 100% noise was added to the weakest NOEs, 10% noise was added to the strongest NOEs, and the noise added to the intermediate NOEs was a linear function between 100% and 10% proportional to the NOE intensity value provided by the simulation. The noise added represents a realistic estimate of the current accuracy with which NOE intensities can be observed using multidimensional homo- and hetero-nuclear spectroscopy.
22. W. A. Hendrickson, *Methods Enzymol.* **115**, 252 (1985); R. Engh and R. Huber, *Acta Crystallogr. Sect. A* **47**, 392 (1991).
23. A. E. Torda, R. M. Scheek, W. F. van Gunsteren, *Chem. Phys. Lett.* **157**, 289 (1989); *J. Mol. Biol.* **214**, 223 (1990).
24. M. Nilges, G. M. Clore, A. M. Gronenborn, *FEBS Lett.* **229**, 317 (1988).
25. T. F. Havel, I. D. Kuntz, G. M. Crippen, *Bull. Math. Biol.* **45**, 665 (1983); J. Kuszewski, M. Nilges, A. T. Brünger, *J. Biomol. NMR* **2**, 33 (1992).
26. A. T. Brünger, *X-PLOR, Version 3.1: A System for X-ray Crystallography and NMR* (Yale Univ. Press, New Haven, CT, 1992).
27. P. Yip and D. A. Case, *J. Magn. Reson.* **83**, 643 (1989).
28. C. M. Oshiro, J. Thomason, I. D. Kuntz, *Biopolymers* **31**, 1049 (1991).
29. Distance bound violations are computed as rms differences between computed distances and d_{upper} (Eq. 2) for distances that are larger than d_{upper}.
30. A complete matrix relaxation technique was used to directly refine the atomic coordinates against the NOE intensity data set (*6, 20, 27*). Relaxation matrix and derivative calculations used a mixing time of 150 ms, $\langle r^{-3}\rangle^{-1/3}$ averaging for methyl groups, uniform isotropic tumbling with a rotational correlation time of 2.3 ns, and a 4 Å cutoff (*20*) for the computation of the relaxation pathways. The target function was E_{NMR2} (Eq. 3).

31. Support by the Howard Hughes Medical Institute (A.T.B.), the National Cancer Institute's Biomedical Supercomputer Center [for computer time (A.T.B.)], and the intramural AIDS Directed Antiviral Program of the Office of the Director of the National Institutes of Health (G.M.C. and A.M.G.) is gratefully acknowledged.

2 April 1993; accepted 8 June 1993

Magnetic Field Signatures Near Galileo's Closest Approach to Gaspra

M. G. Kivelson,* L. F. Bargatze, K. K. Khurana, D. J. Southwood, R. J. Walker, P. J. Coleman, Jr.

Two large magnetic field rotations were recorded by the spacecraft Galileo 1 minute before and 2 minutes after its closest approach to the asteroid Gaspra. The timing and the geometry of the field changes suggest a connection with Gaspra, and the events can be interpreted as the result of the draping of the solar wind field around a magnetospheric obstacle. Gaspra's surface field is inferred to be within an order of magnitude of Earth's surface field, and its magnetic moment per unit mass is in the range observed for iron meteorites and highly magnetized chondrites. The location of the magnetic signatures suggests that perturbations are carried by waves in the magnetosonic-whistler mode with wavelengths between electron and ion gyro radii.

On 29 October 1991, the Galileo spacecraft made its closest approach to the asteroid 951 Gaspra. Gaspra is a small (mean radius ~7 km), oddly shaped body that orbits the sun at a mean distance of 2.2 astronomical units (AU) (*1*). It is classified as an S-type asteroid on the basis of reflectance spectra observed from Earth; the surfaces of these asteroids contain varying proportions of olivine and pyroxene and iron-nickel metal. It is a matter of current debate whether asteroids of this class are the parent bodies of chondritic meteorites or stony-iron meteorites (*1, 2*). The parents of stony-iron meteorites are metal-enriched fragments of asteroids that were chemically differentiated. As indicated by its reflectance spectra, Gaspra is unusually metal- and olivine-rich relative to the other S-class asteroids, suggesting that it is more

M. G. Kivelson and P. J. Coleman, Jr., Department of Earth and Space Sciences and the Institute of Geophysics and Planetary Physics, University of California, Los Angeles, CA 90024.
L. F. Bargatze, K. K. Khurana, R. J. Walker, Institute of Geophysics and Planetary Physics, University of California, Los Angeles, CA 90024.
D. J. Southwood, Department of Physics, Imperial College of Science, Technology, and Medicine, London SW7 2BZ, United Kingdom.

*To whom correspondence should be addressed.

likely a fragment of a differentiated body and, therefore, a potential parent of stony-iron meteorites (*1*). However, no metal-rich material was directly detected in the Galileo images, and most of the surface appeared to be covered with regolith (*1*).

There was little reason to expect that Galileo's magnetometer (3) would detect Gaspra because the point of closest approach was 1600 km, or about 230 Gaspra radii (R_G), away from the asteroid-sun line. Nevertheless, tape recorder resources on the spacecraft were allocated to the fields and particles instruments, and data were acquired in the solar wind for about 2 hours while Galileo was near Gaspra as well as at intermittent intervals totaling 40 min throughout the day. The closest approach occurred at 22:36:40 UT. In normal operation, the Galileo magnetometer provides 4.5 vector field measurements per second. In a plot of 4-s averages of the data recorded during the 50-min interval from 22:15 to 23:05 UT (Fig. 1), the most prominent feature is the pair of field rotations, the first 1 min before and the other 2 min after closest approach. The field magnitude changed very little as the field rotated (*4*).

The geometry of the measured field perturbations is readily understood from projections of the field vectors into two orthogonal planes along the spacecraft trajectory (Fig. 2, A and B). The relatively steady upstream field (the fluctuations are small compared with 2-nT magnitude) was predominantly oriented along the *y* axis, perpendicular to the Gaspra-sun line. As the spacecraft reached the point of closest approach, the vectors rotated toward Gaspra in both projections. The first rotation was followed 3 min later by some rapid variations of field direction, but after less than a minute, it rotated back close to the initial direction and stabilized. A projection of the perturbation field vectors $[\mathbf{B}(t) - \mathbf{B}_0]$ (Fig. 2C) shows that between 22:35:56 and 22:38:32 UT, the perturbations almost point at the sun, as expected for the magnetic signature of an obstacle that is removing momentum from the outward-flowing solar wind.

Field rotations are common features of the unmodified solar wind. During the 2-hour period of nearly continuous data taken near Gaspra, there were three clear rotations very remote from the asteroid. None was abrupt, nor did they rotate the field toward the direction of the solar wind flow. We cannot rule out the possibility that the rotations on which we focus were only fortuitously linked to the Gaspra flyby, but we regard the relation as plausible and interpret the perturbations accordingly. We note, for example, that the rotations seen near Gaspra were in a physically significant direction. The field rotated toward the direction of the solar wind flow (Fig. 2), as it would if a highly conducting magnetized fluid were slowed and diverted about an obstacle near Gaspra's location. If the obstacle is of finite length along the direction of the solar wind, the flow is likely to be somewhat disturbed in the wake region as the field lines "snap back" to their unperturbed orientation. Downstream of the obstacle, the field and the flow return to their upstream configuration (Fig. 2).

We assessed various physical models for the field rotations. One possibility is that near closest approach, Galileo passed from the solar wind into a region dominated by the intrinsic field of Gaspra. This is unlikely, particularly because, after it rotated, the field did not vary in either magnitude or direction as the distance from the body changed. It is more probable that the rotation occurred because of the draping of the interplanetary magnetic field (IMF) over an obstacle, a situation that has parallels (on very different spatial scales) with the way that the IMF drapes over unmagnetized or very weakly magnetized bodies, such as Venus, Mars, or comets (*5*), or over the magnetospheres of magnetized planets, such as Earth or Jupiter (*6*). Two features of the interaction are of quantitative importance: the spatial extent of the perturbed region and the angle from the body at which the signature is first encountered.

To the side of the obstacle, the extent of the disturbed region along the flow-aligned (*x*) direction is typically comparable with the length of the object, much like the disturbed region that develops off to the side of a ship between the bow wave and the stern wake. Near Gaspra, the length of the disturbed region was roughly 1300 km, two orders of magnitude longer than Gas-

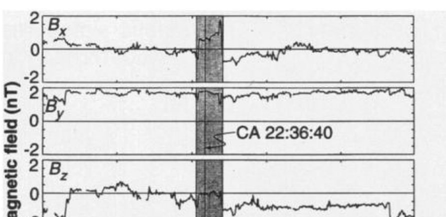

Fig. 1. Three components of the magnetic field and the field magnitude from the Galileo flyby of Gaspra on 29 October 1991. The data have been rotated into a coordinate system in which *x* is the Gaspra-sun line, positive toward the sun, and the average field [$\mathbf{B}_0$ = (0, 2, 0)] before closest approach (CA) (22:30 to 22:32 UT) lies in the *xy* plane. The *z* axis, positive towards ecliptic north, completes the orthogonal triad.

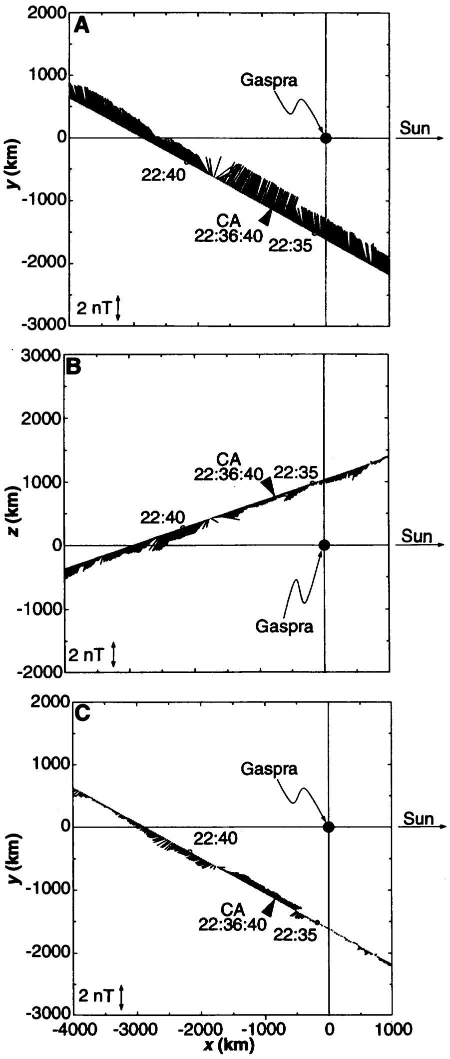

Fig. 2. (**A**) Projections of the magnetic field vectors into the *xy* plane plotted at 4-s intervals along the projected trajectory of the spacecraft. The base of each field vector is set on the trajectory. Gaspra is not drawn to scale. (**B**) Analogous projection in the *xz* plane. (**C**) Plot of perturbation vectors $\mathbf{B}(t) - \mathbf{B}_0$ in *xy* plane.

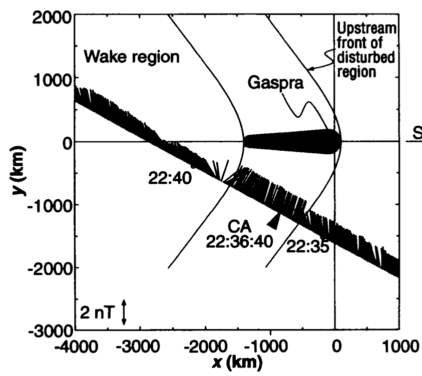

Fig. 3. The projection of Fig. 2A in the *xy* plane with a magnetosphere superimposed. The configuration of the hypothesized fronts that bound the region of disturbance is also illustrated.

pra. This scale suggests that the obstacle was not Gaspra itself but either an asteroid-centered cloud of heavy ions or charged dust or a magnetospheric cavity created by a magnetic field large enough to stand off and divert the solar wind. Outgassing, required to provide a source of heavy ions, seems improbable, and the abrupt return to the unperturbed orientation of the field near 22:40 UT is not what one would expect from a comet-like ion tail that gradually becomes more tenuous downstream of the nucleus. The magnetospheric interaction appears to be the more likely explanation of the flow-aligned extent of the signature. The model has quantitative implications.

Typical magnetospheres start some distance upstream of a planet and extend roughly 10 times that distance downstream; therefore, we estimate that the subsolar point of the putative magnetosphere lies on the x axis between ~30 and ~100 km upstream of Gaspra and the tail of the magnetosphere extends ~1000 km downstream (Fig. 3) (evidently, Galileo would not have penetrated within a magnetosphere of this assumed size). The magnetic moment M_G required to produce the upstream standoff distance R_M can be found from (7)

$$R_M^6 = \kappa\mu_0(M_G/4\pi)^2/2P_{sw} \qquad (1)$$

where μ_0 is the magnetic permeability of vacuum ($4\pi \times 10^{-7}$ henry m^{-1}), the proportionality factor $\kappa = 1.7$ for Earth's magnetosphere, which we take as representative, and P_{sw} is the pressure of the solar wind, dominated by the dynamic pressure ρu^2, where ρ is the mass density of the solar wind, expected to be about 1 atomic mass unit (amu) per cubic centimeter at Gaspra's distance, and u is its velocity, which we take as 400 km s^{-1}. These nominal values will be subject to correction when in situ plasma measurements (8) become available. The inferred magnetic moment is between 6×10^{12} and 2×10^{14} A·m^2, more than eight orders of magnitude smaller than the value for Earth ($M_E = 8 \times 10^{22}$ A·m^2) but large for a body of Gaspra's size. The field at a surface 7 km from the dipole center would be between 0.04×10^{-4} and 1.4×10^{-4} T, a range that includes the value of Earth's surface field at the equator (0.3×10^{-4} T). In such a field, the gyro frequency for electrons is between 100 kHz and 4 MHz, which defines the highest frequencies of Gaspra-related electromagnetic radiation that could be observed by the Galileo plasma wave detector (9).

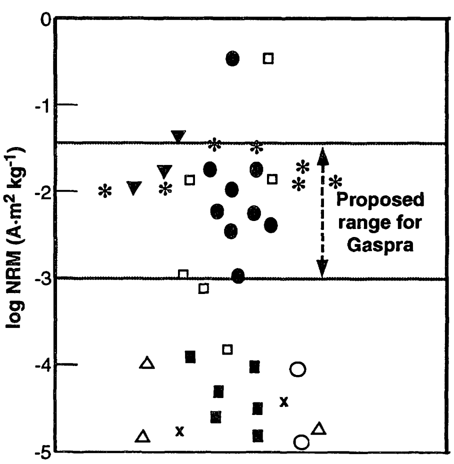

Fig. 4. Natural remanent magnetization (NRM) of meteorites [estimated from figure 8.1.3, A and B, in (10)] and the range estimated for Gaspra's magnetic moment per kilogram. Symbols: (▼) enstatite chondrites, (∗) H chondrites, (●) iron, (□) ureilite, (■) SNC, (×) howardite, (○) eucrite, and (△) diogenite.

Assuming a nominal density of 4000 kg m^{-3} for Gaspra (Galileo's distant flyby, dictated by concerns for safety, was too remote to allow a measurement of the mass of Gaspra), we infer a magnetic moment per unit mass between 0.001 and 0.03 A·m^2 kg^{-1}, which can be compared (Fig. 4) with reported values for differentiated meteorites and chondrites (10). The most strongly magnetized meteorites, such as iron meteorites and metal-rich chondrites, have values that fall within the bounds of the estimates for Gaspra. This is surprising because it implies that the magnetized material of Gaspra is more or less uniformly oriented throughout, which in turn requires that at least most of the body cooled through the Curie temperature while in a large external magnetic field.

These large fields must also have been stable over the time needed for the body to cool through the Curie temperature. Such a stable field could be produced in the mantle or crust of a planet-size body by an internal dynamo. Gaspra might then be a fragment of a differentiated parent body. Alternatively, Gaspra or its parent body may have cooled in a magnetic field capable of aligning ferromagnetic material that was present in the early solar system, a feature that has been proposed in other contexts (11). Consistent with its inferred high olivine and metal abundance, Gaspra might then be a magnetized chondrite.

The fact that the estimated magnetic moment of Gaspra falls in the range observed for strongly magnetized meteorites encourages us to believe that our interpretation of the solar wind disturbance recorded near Gaspra, albeit preliminary, is correct. If so, the relatively high value of the estimated magnetic moment places constraints on the composition and mean density of Gaspra, adding to other evidence that it is metal-rich.

The geometry of the solar wind interaction region can be treated in the magnetohydrodynamic (MHD) limit in the case of planetary bodies whose scale is large compared with ion gyro radii. For protons flowing at the solar wind speed relative to Gaspra, however, the gyro radius is ~2000 km, large compared with both Gaspra and its putative magnetosphere. Solar wind electrons, with gyro radii of ~1 km, remain tied to the magnetic field on the scale of the proposed magnetosphere, and the electron fluid is diverted along with the draping of the field about the obstacle. The boundaries that confine the perturbed portion of the solar wind (shown schematically in Fig. 3) fold back in the direction of the flow because the perturbations propagate at finite wave speeds and are swept back as they move away from the source region (12). The angle between the flow direction and the wave front is roughly the arc tangent of the wave speed divided by the flow speed, but details depend on the specific wave mode that carries the perturbation.

A crude estimate of the relevant wave mode can be obtained from the warm-plasma dispersion relation. We assume that wave power peaks at wavelengths, λ, comparable with the spatial scale of the obstacle in the direction transverse to the flow. That scale is between 100 and 300 km, assuming that the width of the magnetosphere is roughly three times the distance from Gaspra to the subsolar point of the magnetopause. The dispersion relation (13) for these conditions shows that the magnetosonic-whistler branch is pertinent, and this type of wave is what carries the pressure perturbations that slow and divert the flow. With an estimated Alfvén speed (c_A) of 40 km s^{-1} and an ion gyro frequency of 0.03 Hz, appropriate to the measured field of 2 nT and an assumed density of 1 amu cm^{-3}, we estimate the phase and group velocities from the approximation

$$(\omega/k)^2 = c_A^2\ \omega \cos\theta/\Omega_+$$

which is good even in warm plasmas for nearly field-aligned propagation (13). Here k and ω are the wave number and the frequency of the wave, θ is the angle between $\mathbf{k}$ and $\mathbf{B}$, and Ω_+ is the proton gyro frequency. With $\lambda = 2\pi/k$ between 100 and 300 km, the phase velocity is between 180 and 540 km s^{-1} and the group velocity is roughly twice that.

Although the estimate is very crude, it allows us to argue that the upstream front behind which the disturbances are present must make an angle closer to 45° with the Gaspra-sun line than to either 0° or 90° (for planetary magnetospheres, MHD conditions apply, and the disturbance fronts are the bow shocks that make an asymptotic angle of <6° for the assumed solar wind conditions). The double wedge-shaped regions of perturbed solar wind

(Fig. 3) are referred to as whistler wings. The name describes both the structure and the fact that the perturbations are carried in the whistler mode (*14*) [analogous structures in which the perturbations are carried along the magnetic field by Alfvén waves while being swept downstream by a flowing plasma were originally described for the MHD limit (*15*) and were called Alfvén wings]. The perturbation in the whistler mode has to our knowledge been reported only in laboratory experiments. The experiments (*16*) were carried out in a regime for which the spatial scale of the obstacle was small compared with the ion gyro radii and large compared with the electron gyro radii, which corresponds to the circumstances of our measurements [this unusual regime has also been studied in a spacecraft barium release (*17*) but never before in a natural context].

Several other instruments (*8, 9, 18*) on the Galileo spacecraft made in situ measurements that will be useful for improvement of the analysis presented here. Small changes in flow direction linked to the diversion of the flow around the obstacle could possibly be observed by the electron sensors of the Plasma Instrumentation (PLS) (*8*) and the Energetic Particle Detector (EPD) (*18*), although the angular changes are probably too small to be reliably identified. Both instruments may be able to search for a local population of heavy ions to check whether we have been premature in ruling out a comet-like interaction.

It will also be of interest to see if the magnetosonic-whistler waves that carry the pressure perturbations can be detected. The power in these waves is expected to peak at ~3 Hz in the plasma rest frame, but they will be Doppler-shifted by the flow to much lower frequencies in the spacecraft frame. Further work will be needed to extract evidence of these Doppler-shifted waves from the magnetometer data.

If electrons can be trapped in the magnetospheric cavity surrounding Gaspra, they may radiate electromagnetic power near the electron cyclotron frequency, much as electrons at low-altitudes in the Jovian magnetosphere produce ~10-MHz (decametric) emissions (*19*). The inferred magnetic moment of Gaspra constrains the frequencies of such an emission to the band below 100 kHz for the lower estimated magnetic moment and below 4 MHz for the higher estimate. Enhanced power within this range of frequencies in the spectra of the Plasma Wave System (PWS) (*9*) would support the interpretation that we have provided, but initial results do not show any signals.

These observations provide a rationale for outfitting asteroid-bound spacecraft with magnetometers. They also suggest further investigation of the relevant parameter regime in laboratory experiments and computer simulations.

REFERENCES AND NOTES

1. M. J. S. Belton *et al.*, *Science* **257**, 1647 (1992).
2. F. P. Fanale, B. E. Clark, J. F. Bell, *J. Geophys. Res.* **97**, 20863 (1992).
3. M. G. Kivelson *et al.*, *Space Sci. Rev.* **60**, 357 (1992).
4. Because of the 10-month gap in high-resolution data after the flyby of Earth in late 1990, it was necessary to determine the offset for the magnetic field sensor aligned with the spacecraft spin axis from the limited data available at Gaspra. If the wrong offset is used, the magnitude of the field appears to change when the field merely rotates. Because the solar wind magnitude typically changes little across discontinuities, we selected an offset that minimized the variations of the field magnitude in a dataset that did not include the 4 min of data around Gaspra. The variability of the field magnitude associated with the large rotations near closest approach was then small.
5. J. Luhmann *et al.*, *J. Geophys. Res.* **91**, 3001 (1986).
6. T. Ogino, R. J. Walker, M. Ashour-Abdalla, *IEEE Trans. Plasma Sci.* **20**, 487 (1992).
7. R. E. Holzer and J. A. Slavin, *J. Geophys. Res.* **83**, 3831 (1978).
8. L. Frank *et al.*, *Space Sci. Rev.* **60**, 283 (1992).
9. D. Gurnett *et al.*, *ibid.*, p. 341.
10. N. Sugiura and D. W. Strangway, in *Meteorites and the Early Solar System*, J. F. Kerridge and M. S. Matthews, Eds. (Univ. of Arizona Press, Tucson, 1988), pp. 595–615.
11. C. P. Sonett, *Geophys. Res. Lett.* **5**, 151 (1978).
12. J. R. Spreiter and A. Y. Alksne, *Annu. Rev. Fluid Mech.* **2**, 313 (1970).
13. See, for example, V. Formisano and C. F. Kennel, *J. Plasma Phys.* **3**, 55 (1969); T. J. M. Boyd and J. J. Sanderson, *Plasma Dynamics* (Barnes and Noble, New York, 1969), p. 191.
14. E. W. Greenstadt, in *Physical Studies of Minor Planets*, T. Gehrels, Ed. (National Aeronautics and Space Administration SP-267, Washington, DC, 1971), pp. 567–575; *Icarus* **14**, 374 (1971).
15. S. D. Drell, H. M. Foley, M. A. Ruderman, *J. Geophys. Res.* **70**, 3131 (1965).
16. R. L. Stenzel and J. M. Urrutia, *Geophys Res. Lett.* **16**, 361 (1989).
17. H. Luhr *et al.*, *Nature* **320**, 10 (1986).
18. D. J. Williams *et al.*, *Space Sci. Rev.* **60**, 385 (1992).
19. D. A. Gurnett and F. L. Scarf, in *Physics of the Jovian Magnetosphere*, A. J. Dessler, Ed. (Cambridge Univ. Press, New York, 1983), pp. 285–316; T. D. Carr, M. D. Desch, J. K. Alexander, *ibid.*, pp. 226–284.

20. We thank C. Polanskey, T. Johnson, S. Joy, C. F. Kennel, T. King, C. T. Russell, and J. T. Wasson for their essential contributions to this work. We are grateful to the Galileo team at the Jet Propulsion Laboratory (JPL), especially T. Johnson and W. O'Neil. We thank D. Gurnett for providing a preview of the data from his instrument. This work was partially supported by JPL under contract no. 958694.

29 January 1993; accepted 27 May 1993

Experimental Realization of the Covalent Solid Carbon Nitride

Chunming Niu, Yuan Z. Lu, Charles M. Lieber*

Pulsed laser ablation of graphite targets combined with an intense, atomic nitrogen source has been used to prepare C-N thin film materials. The average nitrogen content in the films was systematically varied by controlling atomic nitrogen flux. Rutherford backscattering measurements show that up to 40 percent nitrogen can be incorporated on average into these solids under the present reaction conditions. Photoelectron spectroscopy further indicates that carbon and nitrogen form an unpolarized covalent bond in these C-N materials. Qualitative tests indicate that the C-N solids are thermally robust and hard. In addition, strong electron diffraction is observed from crystallites within the films. Notably, analysis of these diffraction data show that the only viable structure for the C-N crystallites is that of β-C_3N_4, a material predicted theoretically to exhibit superhardness. The experimental synthesis of this new C-N material offers exciting prospects for both basic research and engineering applications.

The development of new materials exhibiting useful mechanical, electronic, or magnetic properties represents a central challenge of materials research (*1*). Among the wide array of important properties, hardness is a material characteristic that may be possible to understand with current theory, and thus it represents an ideal one in which to test our ability to design materials with predictable properties. Because hardness is also one material property that is essential to many high-performance engineering applications, this endeavor is of great technological importance as well (*2*). Hardness can be well represented by the bulk modulus of an ideal solid. Both empirical and ab initio calculations have shown that a large bulk modulus (and corresponding hardness) require short, covalent bonds within a solid (*3, 4*). Notably, it was predicted on the basis of these theoretical ideas that the covalent carbon-nitrogen solid, β-C_3N_4,

C. Niu, Department of Chemistry, Harvard University, Cambridge, MA 02138.
Y. Z. Lu, Materials Research Laboratory, Harvard University, Cambridge, MA 02138.
C. M. Lieber, Department of Chemistry and Division of Applied Sciences, Harvard University, Cambridge, MA 02138.

*To whom correspondence should be addressed.